Precision measurement of the hadronic cross-section through the radiative return method

Germán Rodrigo [a*], Henryk Czyż [b†] and Johann H. Kühn [c‡]

[a]Theory Division, CERN, CH-1211 Geneva 23, Switzerland.

[b]Institute of Physics, University of Silesia, PL-40007 Katowice, Poland.

[c]Institut für Theoretische Teilchenphysik, Universität Karlsruhe, D-76128 Karlsruhe, Germany.

Electron–positron annihilation into hadrons plus an energetic photon from initial-state radiation allows the hadronic cross-section to be measured over a wide range of energies at high luminosity meson factories. Weighted integrals over this cross-section are a decisive input for electroweak precision tests. A Monte Carlo event generator called PHOKHARA has been developed, which simulates $e^+e^- \to$ hadrons + photon(s) at the NLO accuracy. The latest tests and upgrades are presented in this paper.

1. INTRODUCTION

The total cross-section for electron–positron annihilation into hadrons is one of the fundamental observables in particle physics. Its high energy behaviour provides one of the first and still most convincing arguments for the point-like nature of quarks. Its normalization was evidence for the existence of quarks of three different colours, and the recent precise measurements even allow for an excellent determination of the strong coupling at very high [1] and intermediate energies (e.g. [2] and refs. therein) through the influence of QCD corrections.

Weighted integrals over this cross-section with properly chosen kernels are, furthermore, a decisive input for electroweak precision tests. This applies, for example, to the electromagnetic coupling at higher energies or to the anomalous magnetic moment of the muon.

Of remarkable importance for these two applications is the low energy region, say from threshold up to centre-of-mass system (cms) energies of approximately 3 GeV and 10 GeV, respectively. Recent measurements based on energy scans between 2 and 5 GeV have improved the accuracy in part of this range. However, similar, or even further improvements below 2 GeV would be highly welcome. The region between 1.4 GeV and 2 GeV, in particular, is poorly studied and no collider will cover this region in the near future. Improvements or even an independent cross-check of the precise measurements of the pion form factor in the low energy region by the CMD2 and DM2 collaborations would be extremely useful, in particular in view of the disagreement found with the analysis based on isospin-breaking-corrected τ decays [3]. Since this dominates in the analysis of the muon anomalous magnetic moment, this kind of studies will help to clarify the situation with respect to the experimental measurement [4] of this quantity.

2. RADIATIVE RETURN AT MESON FACTORIES

Experiments at present electron–positron colliders operate mostly at fixed energies, albeit with enormous luminosity, with BABAR and BELLE at 10.6 GeV, CLEO-C in the region between 3 and 5 GeV, and KLOE at 1.02 GeV as most prominent examples.

This peculiar feature allows the use of the ra-

diative return, i.e. the reaction

$$e^+(p_1)+e^-(p_2) \rightarrow \gamma(k_1)+\gamma^*(Q)(\rightarrow \text{hadrons}) \,, (1)$$

to explore a wide range of Q^2 in a single experiment [5,6,7,8,9,10].

Nominally an invariant mass of the hadronic system between $2m_\pi$ and the cms energy of the experiment is accessible. In practice, to clearly identify the reaction, it is useful to consider only events with a hard photon — tagged or untagged — which lowers the energy significantly.

The study of events with photons emitted under both large and small angles, and thus at a significantly enhanced rate, is particularly attractive for the $\pi^+\pi^-$ final state with its clear signature, an investigation performed at present at DAΦNE [11,12,13,14]. Events with a tagged photon, emitted under a large angle with respect to the beam, have a clear signature and are thus particularly suited to the analysis of hadronic final states of higher multiplicity [15].

3. MONTE CARLO SIMULATION

To arrive at reliable predictions including kinematical cuts as employed by realistic experiments, a Monte Carlo generator is indispensable. The inclusion of radiative corrections in the generator and the analysis is essential for the precise extraction of the cross-section. For hadronic states with invariant masses below 2 or even 3 GeV, it is desirable to simulate the individual exclusive channels with two, three, and up to six mesons, i.e. pions, kaons, etas, etc., which requires a fairly detailed parametrization of the various form factors.

A first program, called EVA, was constructed some time ago [5] to simulate the production of a pair of pions together with a hard photon. It includes initial-state radiation (ISR), final-state radiation (FSR), their interference, and the dominant radiative corrections from additional collinear radiation through structure function (SF) techniques [16]. This project was continued with the construction of a generator for the radiative production of four pions [7].

As a further development of this project a new Monte Carlo generator called PHOKHARA [17]
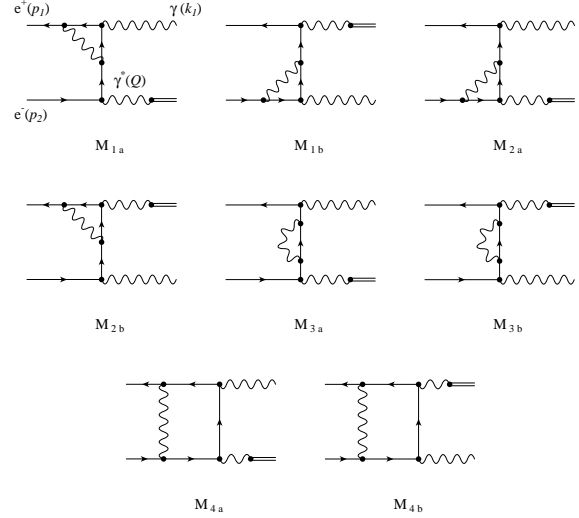

Figure 1. One-loop corrections to initial-state radiation in $e^+e^- \rightarrow \gamma+$ hadrons.

has been constructed, which includes, in contrast to the former generators, the complete next-to-leading order (NLO) radiative corrections. The first version of PHOKHARA incorporates ISR only and is limited to $\pi^+\pi^-\gamma(\gamma)$ and $\mu^+\mu^-\gamma(\gamma)$ as final states. PHOKHARA exhibits a modular structure that simplifies the implementation of additional hadronic modes or the replacement of the currents(s) of the existing modes.

In this paper we show how PHOKHARA is constructed and present some results obtained with its current version, as well as a comparison with the other aforementioned generators. Finally, the new features that will be part of the next version of PHOKHARA are outlined and some preliminary results are presented. Further details will be given, however, in a forthcoming publication [18]. These programs and the future versions of PHOKHARA can be downloaded from `http://cern.ch/german.rodrigo/phokhara/`.

4. NLO CORRECTIONS TO ISR

At NLO, the e^+e^- annihilation process (1), where the virtual photon converts into a hadronic final state, $\gamma^*(Q) \rightarrow$ hadrons, and the real one is emitted from the initial state, receives contribu-
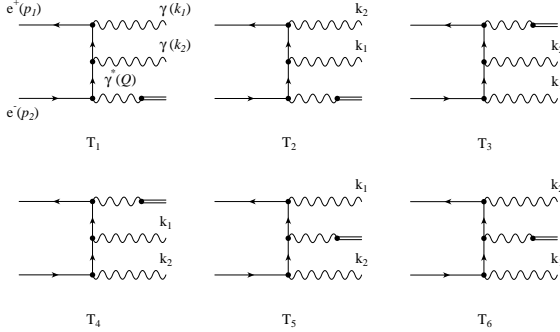
Figure 2. Emission of two real photons from the initial state in e^+e^- annihilation into hadrons.

tions from one-loop corrections (see Fig. 1) and from the emission of a second real photon (see Fig. 2).

After renormalization the one-loop matrix elements still contain infrared divergences. These are cancelled by adding the contribution where a second photon has been emitted from the initial state. This rate is integrated analytically in phase space up to an energy cutoff $E_\gamma < w\sqrt{s}$ far below $\sqrt{s}$. The sum is finite; however, it depends on this soft photon cutoff. The contribution from the emission of a second photon with energy $E_\gamma > w\sqrt{s}$ completes the calculation and cancels this dependence.

In order to facilitate the extension of the Monte Carlo simulation to different hadronic exclusive channels, the differential rate for the virtual and soft QED corrections is cast into the product of a leptonic and a hadronic tensor and the corresponding factorized phase space:

$$
\begin{aligned}
d\sigma &= \frac{1}{2s} \, L_{\mu\nu} \, d\Phi_2(p_1, p_2; Q, k_1) \\
&\times \quad H^{\mu\nu} \, d\Phi_n(Q; q_1, \cdot, q_n) \, \frac{dQ^2}{2\pi} \;,
\end{aligned} \tag{2}
$$

where $d\Phi_n(Q; q_1, \cdot, q_n)$ denotes the hadronic n-body phase space including all statistical factors and Q^2 is the invariant mass of the hadronic system.

The physics of the hadronic system, whose description is model-dependent, enters only through the hadronic tensor

$$
H^{\mu\nu} = J^\mu J^{\nu+} \;, \tag{3}
$$

where the hadronic current has to be parametrized through form factors [7,19,20,21].

The leptonic tensor, which describes the NLO virtual and soft QED corrections to initial-state radiation in e^+e^- annihilation, has the following general form:

$$
\begin{aligned}
L^{\mu\nu} &= \frac{(4\pi\alpha)^2}{Q^4} \left[a_{00} \, g^{\mu\nu} + a_{11} \, \frac{p_1^\mu p_1^\nu}{s} \right. \\
&+ \quad a_{22} \frac{p_2^\mu p_2^\nu}{s} + a_{12} \frac{p_1^\mu p_2^\nu + p_2^\mu p_1^\nu}{s} \\
&+ \quad \left. i\pi \, a_{-1} \frac{p_1^\mu p_2^\nu - p_2^\mu p_1^\nu}{s} \right] \;.
\end{aligned} \tag{4}
$$

Terms proportional to Q^μ are absent as a consequence of current conservation. The scalar coefficients a_{ij} and a_{-1} allow the following expansion

$$
a_{ij} = a_{ij}^{(0)} + \frac{\alpha}{\pi} \, a_{ij}^{(1)} \;, \qquad a_{-1} = \frac{\alpha}{\pi} \, a_{-1}^{(1)} \;, \tag{5}
$$

where $a_{ij}^{(0)}$ provide the leading order (LO) contribution and the imaginary antisymmetric piece proportional to a_{-1} appears for the first time at NLO.

As an alternative one can replace the Cartesian basis (4) by a basis derived from the three circular polarization vectors of the virtual photon ε_L and $\varepsilon_\pm$:

$$
L^{\mu\nu} = \frac{(4\pi\alpha)^2}{Q^4} \sum a_{ij} \, \varepsilon_i^{*\mu} \varepsilon_j^\nu \;, \quad i,j = L,\pm \;, \tag{6}
$$

where only four of the scalar coefficients are independent

$$
\begin{aligned}
a_{L-} &= a_{L+} \;, & a_{-L} &= a_{+L} = a_{L+}^* \;, \\
a_{--} &= a_{++} \;, & a_{-+} &= a_{+-} \;.
\end{aligned}
$$

An expansion similar to (5) holds for these scalar coefficients. The relationship between the components in both bases as well as expressions for these coefficients can be found in [22,23]. The trace of the leptonic tensor, which is related to the cross-section after angular averaging of the hadronic tensor, is particularly simple in the second case:

$$
L^{\mu\nu}(Q_\mu Q_\nu - g_{\mu\nu} Q^2) = \frac{(4\pi\alpha)^2}{Q^2}(a_{LL} + 2a_{++}) \;. \tag{7}
$$

Note that the imaginary part of $L_{\mu\nu}$, which is present in the coefficients a_{L+} or a_{-1} only, is of interest for those cases where the hadronic current receives contributions from different amplitudes with non-trivial relative phases. This is possible, e.g. for final states with three or more mesons or for $p\bar{p}$ production.

The matrix elements for the emission from the initial state of two real hard photons, i.e. $E_\gamma > w\sqrt{s}$,

$$e^+(p_1) + e^-(p_2) \rightarrow \gamma^*(Q) + \gamma(k_1) + \gamma(k_2) \ , \quad (8)$$

are calculated numerically following the helicity-amplitude method with the conventions introduced in [24,25]. As a test, the square of this matrix element averaged over initial particle polarization has also been calculated using the standard trace technique and tested numerically against the helicity method result.

The virtual plus soft contribution and the hard one depend separately on the soft photon cut-off w used to regulate the infrared divergences of the virtual diagrams. The former shows a logarithmic w dependence. The second, after numerical integration in phase space, exhibits the same behaviour, whereas their sum must be independent of w. To explicitly demonstrate this w-independence is therefore a basic test of the program. Then the value of w that optimizes the event generation, avoiding at the same time the appearance of unphysical negative weights, is determined.

Table 1 presents the total cross-section for radiative production of a pair of pions calculated for several values of the soft photon cutoff at three different cms energies for the kinematical cuts from Table 2. The excellent agreement, within the error of the numerical integration, confirms the w-independence of the result. A value around $w = 10^{-4}$ seems to be the best choice [17].

5. LL VERSUS NLO

The original and default version of EVA [5], simulating the process $e^+e^- \rightarrow \pi^+\pi^-\gamma$ at LO, allowed for additional initial-state radiation of soft and collinear photons by the structure-function method [16]. By convoluting the Born cross-
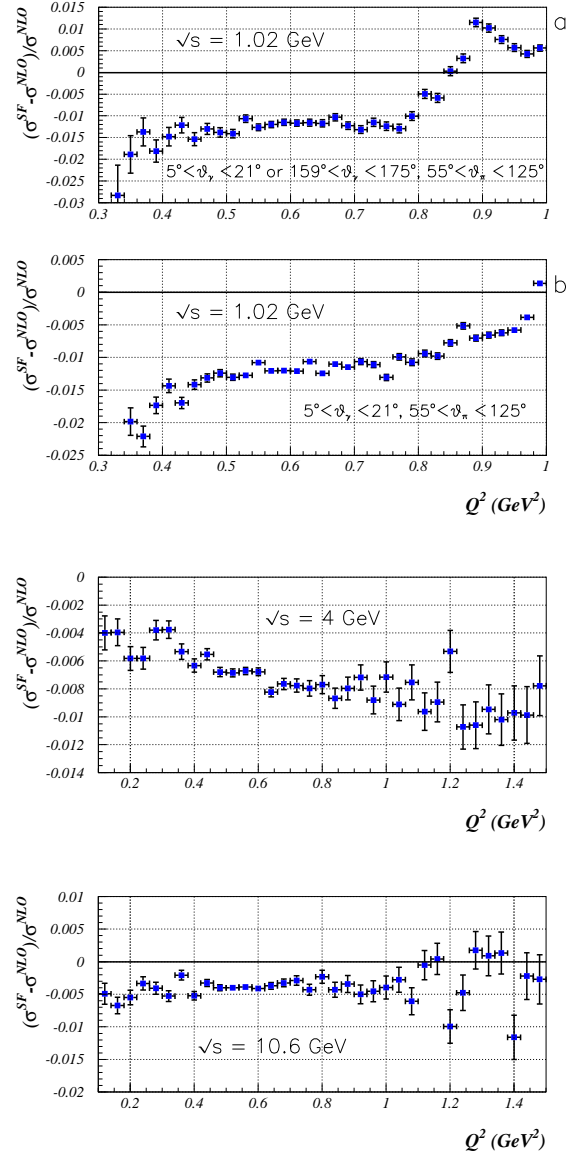

Figure 3. Comparison between the collinear approximation by structure functions and the fixed-order NLO result for different cms energies. Cuts from Table 2.

Table 1

Total cross-section (nb) for the process $e^+e^- \to \pi^+\pi^-\gamma$ at NLO for different values of the soft photon cutoff. Only initial-state radiation. Cuts from Table 2.

w	$\sqrt{s} =$1.02 GeV	4 GeV	10.6 GeV
10^{-3}	2.0324 (4)	0.12524 (5)	0.010564 (4)
10^{-4}	2.0332 (5)	0.12526 (5)	0.010565 (4)
10^{-5}	2.0333 (5)	0.12527 (5)	0.010565 (5)

Table 2

Kinematical cuts applied at different cms energies: minimal energy of the tagged photon ($E_\gamma^{\min}$), angular cuts on the tagged photon (θ_γ) and the pions (θ_π), and minimal invariant mass of the hadrons plus the tagged photon ($M_{\pi^+\pi^-\gamma}^2$)

	$\sqrt{s} =$1.02 GeV	4 GeV	10.6 GeV
$E_\gamma^{\min}$ (GeV)	0.01	0.1	1
θ_γ (degrees)	$[5, 21]$	$[10, 170]$	$[25, 155]$
θ_π (degrees)	$[55, 125]$	$[20, 160]$	$[30, 150]$
$M_{\pi^+\pi^-\gamma}^2$ (GeV^2)	0.9	12	90

Table 3

Total cross-section (nb) for the process $e^+e^- \to \pi^+\pi^-\gamma$ at LO, NLO and in the collinear approximation via structure functions (SF), with the cuts from Table 2. Only initial-state radiation. NLO(2) gives the NLO result with the same cuts as NLO(1) but for the hadron–photon invariant mass unbounded.

	$\sqrt{s} =$1.02 GeV	4 GeV	10.6 GeV
Born	2.1361 (4)	0.12979 (3)	0.011350 (3)
SF	2.0192 (4)	0.12439 (5)	0.010526 (3)
NLO (1)	2.0332 (5)	0.12526 (5)	0.010565 (4)
NLO (2)	2.4126 (7)	0.14891 (9)	0.012158 (9)

Table 4

Total cross-section (nb) for initial-state radiation in the process $e^+e^- \to \mu^+\mu^-\gamma$ at LO, NLO (1) and NLO (2) with the cuts from Table 2, the pions being replaced by muons.

	$\sqrt{s} =$1.02 GeV	4 GeV	10.6 GeV
Born	0.8243(5)	0.4690(6)	0.003088(6)
NLO (1)	0.7587(5)	0.4449(6)	0.002865(6)
NLO (2)	0.8338(7)	0.4874(14)	0.00321(6)

Table 5

Total cross-section (nb) for the process $e^+e^- \rightarrow \pi^+\pi^-\gamma$ at $\sqrt{s}$ =1.02 GeV in NLO and in the collinear approximation (SF) as a function of the cut on the invariant mass of the hadron + tagged photon $M^2_{\pi^+\pi^-\gamma}$. Only initial-state radiation. Minimal energy of the tagged photon and angular cuts from Table 2.

$M^2_{\pi^+\pi^-\gamma}$ (GeV^2)	SF	NLO
0.1	2.4127(18)	2.4132(8)
0.2	2.4126(18)	2.4131(8)
0.3	2.4124(18)	2.4127(8)
0.4	2.4098(18)	2.4096(8)
0.5	2.3949(18)	2.3953(8)
0.6	2.3425(16)	2.3455(8)
0.7	2.2449(11)	2.2543(8)
0.8	2.1387(9)	2.1533(8)
0.9	2.0198(8)	2.0334(8)
0.95	1.9437(8)	1.9522(8)
0.99	1.8573(8)	1.8559(8)

section with a given SF distribution, soft photons are resummed to all orders in perturbation theory and large logarithms of collinear origin, $L = \log(s/m_e^2)$, are taken into account up to two-loop approximation. The NLO result, being a complete one-loop result, contains these logarithms in order α and additional subleading terms, which of course are not taken into account within the SF method. Although small, these subleading contributions become important for measurements aiming at an accuracy better than 1%. Furthermore, a NLO generator is more suitable for comparison with an experimental setup. While in the SF approach the extra collinear photon emission is integrated out and some information is lost, in a fixed-order calculation the full angular dependence is kept and energy-momentum is conserved, i.e. the sum of the momenta of the generated outgoing particles agrees with the incoming e^+e^- momentum.

Table 3 presents the total cross-section for $e^+e^- \rightarrow \pi^+\pi^-\gamma(\gamma)$ calculated at LO and NLO for three different cms energies with the kinematical cuts listed in Table 2. Two NLO predictions are shown. The first one, NLO(1), which can be compared with the SF result derived from EVA, includes a cut on the invariant mass of the hadrons plus the tagged photon. The last was introduced in [5] in order to reduce the kinematic distortion of the events due to the extra collinear emission. The second prediction, NLO(2), is obtained without this cut. The Q^2 dependence of the difference between the NLO(1) prediction and the SF result is showed in Fig. 3. The size and sign of the NLO corrections do depend on the particular choice of the experimental cuts. Hence only using a Monte Carlo event generator can one realistically compare theoretical predictions with experiment and extract $R(s)$ from the data.

The results of EVA and those denoted NLO(1) for the total cross-section are in reasonably good agreement. Both of them are clearly sensitive to the cut on $M^2_{\pi^+\pi^-\gamma}$. This cut dependence is displayed in Table 5. Remarkably, the typical difference between the results of the two programs is clearly less than 0.5% for most of the entries.

The systematic uncertainty of the program, due to inadequate treatment of ISR, namely missing leading logarithmic higher order corrections and lepton pair production, is conservatively estimated to be of around 0.5% in the total cross-section [17].

6. MUON PAIR PRODUCTION

Results for the total cross-section of muon pair production are listed in Table 4. The radiative muon cross-section can be used for a calibration of the pion yield. A number of radiative corrections are expected to cancel in the ratio. For this reason we consider the ratio between the pion and the muon yields, after dividing the former by $|F_\pi(Q^2)|^2(1 - 4m_\pi^2/Q^2)^{3/2}$, the latter by $4(1 + 2m_\mu^2/Q^2)\sqrt{1 - 4m_\mu^2/Q^2}$. In Fig. 4a we consider the full angular range for pions and muons, with θ_γ between 5° and 21°. Clearly all radiative corrections and kinematic effects disappear, up to statistical fluctuations, in the leading order program as well as after inclusion of the NLO corrections.
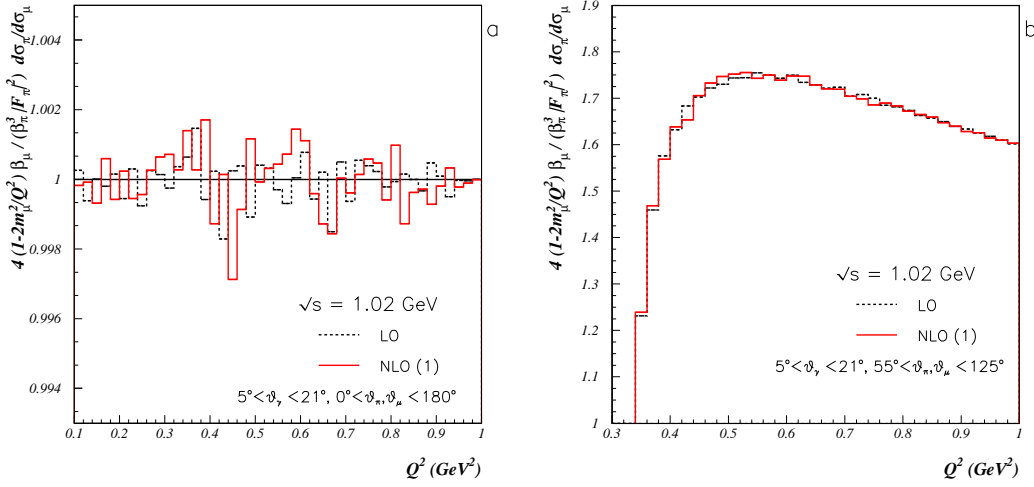
In Fig. 4b an additional cut on pion and muon

Figure 4. Ratio between pion and muon yields, after dividing through their respective R-ratio. a: no cuts on pion and muon angles; b: with angular cuts on pion and muon angles.

angles has been imposed. As demonstrated in Fig. 4b, the ratio differs from unity once (identical) angular cuts are imposed on pions and muons, a consequence of their different angular distribution. To derive the pion form factor from the ratio between pion and muon yields, this effect has to be incorporated. However, the correction function shown in Fig. 4b is independent from the form factor, and hence universal and model-independent (ignoring FSR for the moment).

7. UNTAGGED PHOTONS

Both EVA and PHOKHARA were initially designed to simulate reactions with tagged photons, i.e. at least one photon was required to be emitted under large angles. The extension of these results to untagged photon events, i.e. for photons emitted at arbitrary small angles, was recently investigated [23,26].

An important ingredient in the extension of the NLO Monte Carlo program PHOKHARA to small photon angles is the evaluation of the virtual corrections to reaction (1) in the limit $m_e^2/s \ll 1$, which are equally valid for large and small angles. Compact results for the one-loop two-, three- and four-point functions that enter this calculation can be found in the litera-
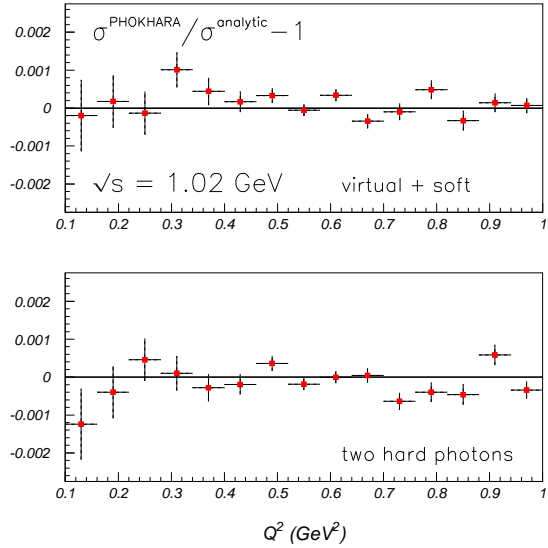

Figure 5. Comparison of the virtual+soft and hard contributions to the $\pi^+\pi^-$ differential cross-section with inclusive analytical results. Soft photon cutoff: $w = 10^{-4}$.
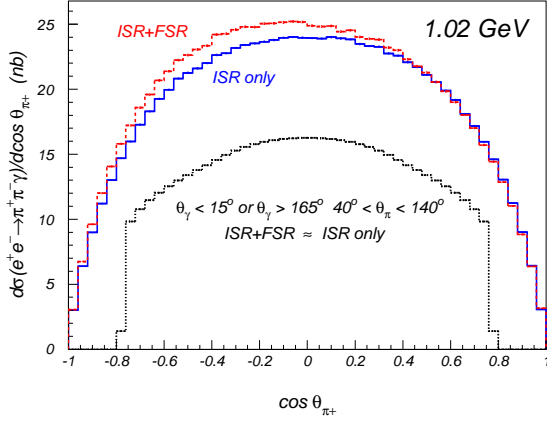
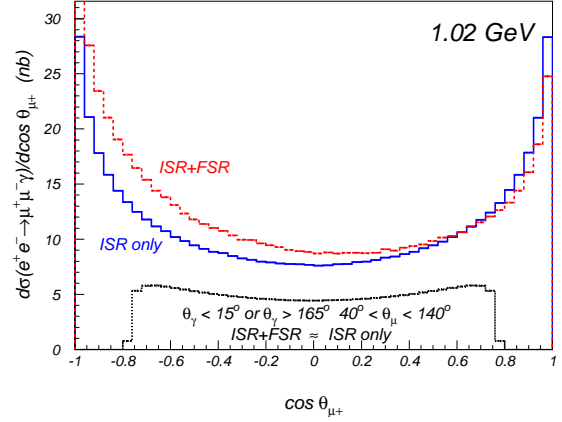Figure 6. Angular distribution of π^+ with and without FSR for different angular cuts.

Figure 7. Angular distribution of μ^+ with and without FSR for different angular cuts.

ture [27,28] for arbitrary values of m_e^2/s. However, the combination of these analytical expressions with the relevant coefficients is numerically unstable in the limit of small mass and angles. A compact, numerically stable result, valid for an arbitrarily small photon angle, is therefore required. As a consequence of the highly singular kinematic coefficients, terms proportional to m_e^2 and even m_e^4 must be kept in the expansion, which will contribute, after angular integration, to the total cross-section even in the limit $m_e^2/s \to 0$.

Inclusive NLO calculations can be used to test the performance of the simulation at small angles. Figure 5 shows the comparison of the differential cross-section for the $\pi^+\pi^-$ mode with the analytical results from [29,30]. The agreement is excellent.

8. ISR DOMINANCE AND FSR

Final-state radiation should be regarded as the background of the measurement and would be required for the complete simulation of the reaction. The complete leading order matrix element squared is given by

$$|\mathcal{M}|^2 = |\mathcal{M}_{\mathrm{ISR}}|^2 + |\mathcal{M}_{\mathrm{FSR}}|^2 + 2\mathrm{Re}[\mathcal{M}_{\mathrm{ISR}}\mathcal{M}_{\mathrm{FSR}}^\dagger] \,. \quad (9)$$

FSR and its interference with ISR were already included in EVA [5] for the two-pion case. The pions were assumed to be point-like, and scalar

QED was applied to simulate photon emission off the charged pions. There it was demonstrated that suitably chosen configurations, namely those with hard photons at small angles relative to the beam and well separated from the pions, are dominated by ISR. FSR can therefore be reduced to a reasonable limit or be controlled by the simulation.

At B-factories, where one has to deal with very hard tagged photons, the situation is even better because the kinematic separation between the photon and the hadrons becomes very clear. For events where hadrons and photon are produced mainly back to back the suppression of FSR is naturally accomplished.

The third term in the right-hand side of Eq. (9), the ISR–FSR interference, is odd under charge conjugation and its contribution vanishes under angular integration. It gives rise, however, to a relatively large charge asymmetry and, correspondingly, to a forward–backward asymmetry

$$A(\theta) = \frac{N^{\pi^+}(\theta) - N^{\pi^+}(\pi - \theta)}{N^{\pi^+}(\theta) + N^{\pi^+}(\pi - \theta)} \,. \quad (10)$$

The asymmetry can be used for calibration of the FSR amplitude, and fits to the angular distribution $A(\theta)$ can test details of its model dependence.

This is illustrated in Figs. 6 and 7, where the angular distributions of π^+ and μ^+ respectively are shown for different kinematical cuts. The
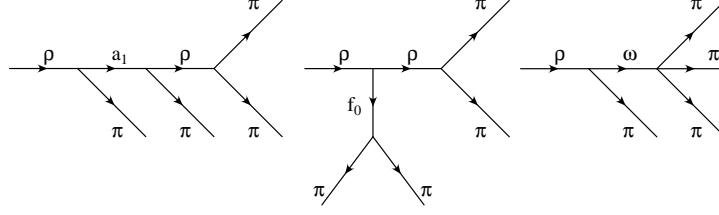
Figure 8. Diagrams contributing to the 4π hadronic current.

angles are defined with respect to the incoming positron. If no angular cut is applied the angular distribution in both cases is highly asymmetric as a consequence of the ISR–FSR interference contribution. If cuts suitable to suppress FSR, and therefore the ISR–FSR interference, are applied the distributions become symmetric. These plots have been obtained with the new version of PHOKHARA, which now incorporates at LO FSR, and its interference with ISR, for two pions (point-like) and muons.

9. NEW HADRONIC CHANNELS

Because of the modular structure of PHOKHARA additional hadronic modes can be easily implemented. The four-pion channels $(2\pi^+2\pi^-$ and $2\pi^0\pi^+\pi^-)$, which give the dominant contribution to the hadronic cross-section in the region from 1 to 2 GeV, are a new feature of our event generator.

Isospin invariance relates the amplitudes of the $e^+e^- \to 2\pi^+2\pi^-$ and $e^+e^- \to 2\pi^0\pi^+\pi^-$ processes and those for τ decays into $\pi^-3\pi^0$ and $\pi^+2\pi^-\pi^0$. The description of the four-pion hadronic current follows [7,20]. The basic building blocks of this current are schematically depicted in Fig. 8 and described in detail in [7].

Results obtained with PHOKHARA for this channel have been compared with the Monte Carlo, which simulates the same process at LO [7] and includes additional collinear radiation through SF techniques. Typically, differences of order 1% are found (see Fig. 9), which are of the expected size and of the same order as for the two-pion final state [17]. Details of the compari-
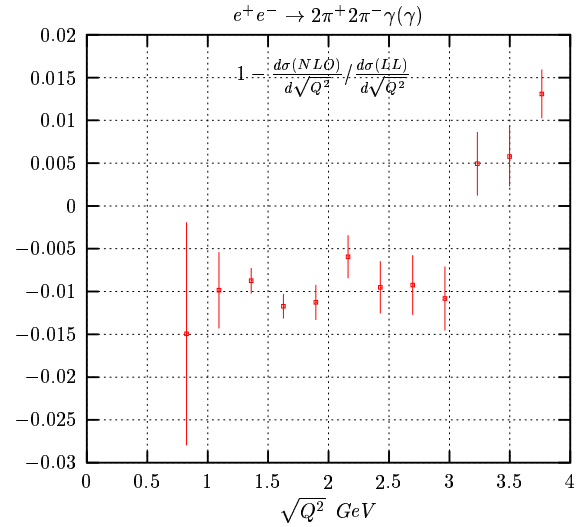
Figure 9. Relative non-leading contribution to the four pion differential cross-section at $\sqrt{s}$=4 GeV.

son and of the performed tests will be presented in a forthcoming publication [18].

The implementation of the three-pion mode is under way. Other hadronic channels will be likewise considered in the future.

10. CONCLUSIONS

The PHOKHARA Monte Carlo event generator has been upgraded. It now includes, besides the $\pi^+\pi^-$ and $\mu^+\mu^-$ channels, also $2\pi^+2\pi^-$ and $2\pi^0\pi^+\pi^-$ as final states. FSR, and its interference with ISR, have also been included for the first two channels. Furthermore, the simulation

of events where the photon(s) is emitted under small angles with respect to the beam axis has been tested numerically. Further upgrades are in progress.

ACKNOWLEDGEMENTS

REFERENCES

1. LEP Collaborations, hep-ex/0103048.
2. J. H. Kühn and M. Steinhauser, Nucl. Phys. B **619** (2001) 588 [hep-ph/0109084].
3. M. Davier, S. Eidelman, A. Höcker and Z. Zhang, hep-ph/0208177. A. Höcker, these proceedings.
4. G. W. Bennett *et al.* [Muon g-2 Collaboration], Phys. Rev. Lett. **89** (2002) 101804 [hep-ex/0208001]. L. Roberts, these proceedings.
5. S. Binner, J. H. Kühn and K. Melnikov, Phys. Lett. **B459** (1999) 279 [hep-ph/9902399].
6. K. Melnikov, F. Nguyen, B. Valeriani and G. Venanzoni, Phys. Lett. **B477** (2000) 114 [hep-ph/0001064].
7. H. Czyż and J. H. Kühn, Eur. Phys. J. C **18** (2001) 497 [hep-ph/0008262].
8. S. Spagnolo, Eur. Phys. J. C **6** (1999) 637.
9. V. A. Khoze, M. I. Konchatnij, N. P. Merenkov, G. Pancheri, L. Trentadue and O. N. Shekhovzova, Eur. Phys. J. C **18** (2001) 481 [hep-ph/0003313]; Eur. Phys. J. C **25** (2002) 199 [hep-ph/0202021].
10. A. Höfer, J. Gluza and F. Jegerlehner, Eur. Phys. J. C **24** (2002) 51 [hep-ph/0107154].
11. G. Venanzoni [KLOE Collaboration], hep-ex/0210013, these proceedings.
12. A. Aloisio *et al.* [KLOE Collaboration], hep-ex/0107023.
13. A. Denig *et al.* [KLOE Collaboration], eConf **C010430** (2001) T07 [hep-ex/0106100].
14. M. Adinolfi *et al.* [KLOE Collaboration], hep-ex/0006036.
15. E. P. Solodov [BABAR collaboration], eConf **C010430** (2001) T03 [hep-ex/0107027].
16. M. Caffo, H. Czyż and E. Remiddi, Nuovo Cim. A **110** (1997) 515 [hep-ph/9704443]; Phys. Lett. **B327** (1994) 369.
17. G. Rodrigo, H. Czyż, J. H. Kühn and M. Szopa, Eur. Phys. J. C **24** (2002) 71 [hep-ph/0112184]. G. Rodrigo, H. Czyż and J. H. Kühn, hep-ph/0205097.
18. H. Czyż, A. Grzelińska, J. H. Kühn and G. Rodrigo, in preparation.
19. J. H. Kühn and A. Santamaria, Z. Phys. C **48** (1990) 445.
20. R. Decker, M. Finkemeier, P. Heiliger and H. H. Jonsson, Z. Phys. C **70** (1996) 247 [hep-ph/9410260].
21. G. Ecker and R. Unterdorfer, Eur. Phys. J. C **24** (2002) 535 [hep-ph/0203075].
22. G. Rodrigo, A. Gehrmann-De Ridder, M. Guilleaume and J. H. Kühn, Eur. Phys. J. C **22** (2001) 81 [hep-ph/0106132].
23. J. H. Kühn and G. Rodrigo, Eur. Phys. J. C **25** (2002) 215 [hep-ph/0204283].
24. F. Jegerlehner and K. Kołodziej, Eur. Phys. J. C **12** (2000) 77 [hep-ph/9907229].
25. K. Kołodziej and M. Zrałek, Phys. Rev. D **43** (1991) 3619.
26. G. Rodrigo, Acta Phys. Polon. B **32** (2001) 3833 [hep-ph/0111151].
27. G. 't Hooft and M. J. Veltman, Nucl. Phys. B **153** (1979) 365.
28. W. Beenakker and A. Denner, Nucl. Phys. B **338** (1990) 349.
29. F. A. Berends, G. J. Burgers and W. L. van Neerven, Phys. Lett. **B177** (1986) 191.
30. F. A. Berends, W. L. van Neerven and G. J. Burgers, Nucl. Phys. **B297** (1988) 429.